Erschienen in: Proceedings of the 28th European Photovoltaic Solar Energy Conference and Exhibition (EU PVSEC 2013) ; Paris, France ; conference 30 September - 04 October 2013. - München : WIP, 2013. - S. 1367-1370. - ISBN 3-936338-33-7
https://dx.doi.org/10.4229/28thEUPVSEC2013-2BV.2.50

ELECTRICAL AND OPTICAL ANALYSIS OF DIELECTRIC LAYERS FOR ADVANCED PASSIVATION OF BBr_3 DIFFUSED P^+ EMITTERS IN N-TYPE C-SI SOLAR CELLS

Joachim H. Ranzmeyer, Yvonne Schiele, Giso Hahn, Barbara Terheiden
University of Konstanz, Department of Physics, 78457 Konstanz, Germany
Phone: +49 (0) 7531 88 4995, Fax: +49 (0) 7531 88 3895
Email: joachim.ranzmeyer@isc-konstanz.de, yvonne.schiele@uni-konstanz.de

ABSTRACT: Due to a different surface concentration and type of minority charge carriers compared to n^+ emitters (on p-type substrates), novel surface passivation methods are required when using p^+ emitters on n-type silicon for which a number of efficiency records have been achieved in recent years [1,2,3]. In this study emitter saturation current densities j_{0e} of two BBr_3 diffused emitters passivated by a variety of dielectric stacks are compared using following processes: SiO_x by dry thermal oxidation, direct and remote plasma enhanced chemical vapor deposited SiN_x, atomic layer deposited Al_2O_3, SiO_x remaining from the RCA standard cleaning process [4] yielding the lowest j_{0e} of 17.5 fA/cm² for a sample passivated by an Al_2O_3/SiN_x stack. Furthermore, the j_{0BSF} values of $POCl_3$ diffused n^+ surfaces passivated by several passivation layers are determined as they are applied at the solar cell rear side. The resulting combined j_{0e} and j_{0BSF} values $j_{0combined}$ are compared with IV characteristics of solar cells passivated by the corresponding passivation of emitter and BSF on front- and rear side. As passivation layers are additionally employed as antireflection coatings also the spectral reflectance of the investigated passivation stacks with optimized thickness was determined.
Keywords: Boron, c-Si, n-type, Passivation

1 INTRODUCTION

n-type silicon has received increasing interest as substrate material for solar cells since it features higher bulk charge carrier lifetimes than p-type doped silicon due to a lower impact of metal impurities like e.g. Fe [5]. In addition, solar cells from n-type Si material do not suffer from light induced degradation due to boron-oxygen complexes [6].

The different structure with p^+-emitter on the front side and the n^+-type doped rear side requires a sophisticated way of surface passivation whose properties matches to minority charge carrier type and surface concentration on both front- and rear side, respectively, in order to achieve highest solar cell efficiencies. Additionally, the front side passivation layer thickness needs to be optimized due to its further use as antireflection coating (ARC) requiring knowledge of the wavelength dependent refractive index n as well as the absorption coefficient k.

In this study, several promising dielectric layers and stacks are investigated as passivation on two different BBr_3 diffused emitters with sheet resistivities of 50 Ω/sq and 100 Ω/sq (see also [7]): silicon nitride applied by direct plasma enhanced chemical vapor deposition (PECVD), stacks composed of atomic layer deposited (ALD) Al_2O_3 + remote-plasma enhanced chemical vapor deposition (r-PECVD) SiN_x, SiO_x by dry thermal oxidation + PECVD-SiN_x and SiO_x remaining from the RCA standard cleaning process (RCA-SiO_x) + PECVD-SiN_x. Additionally, passivation properties of PECVD-SiN_x, thermal SiO_x + PECVD-SiN_x and RCA2-SiO_x + PECVD-SiN_x are investigated on a 60 Ω/sq n^+ $POCl_3$ diffused back-surface-field (BSF) and the combined saturation current densities $j_{0combined} = j_{0e} + j_{0BSF}$ are compared with IV characteristics of solar cells featuring the corresponding emitter/passivation combinations on front- and rear side, respectively.

2 EXPERIMENTAL

To investigate the electrical properties of the investigated passivation/emitter combinations, emitter saturation current densities are determined by the method of Kane and Swanson [8] at an injection level of 1×10^{16} cm^{-3}. For these samples, n-type float zone Si substrates with a base resistivity of 7.5 Ωcm, a thickness of 250 µm and an area of 50 × 50 mm² are used. Emitter as well as passivation layers are applied on both surfaces as required by the method. The samples are divided into three groups, group 1 and group 2 are for measuring j_{0e} of the passivated BBr_3 emitters while the samples of group 3 are for determining j_{0BSF} of the passivated $POCl_3$ diffused n^+ BSFs. Group 1 and 3 are textured in an alkaline solution leading to pyramid textured surfaces with (111) orientation as also applied for solar cells, group 2 has (100) oriented planar surfaces.

The pre-treatment includes a cleaning step in diluted HCl and a subsequent dip in a HF solution after which group 3 samples are directly subjected to a $POCl_3$ diffusion for a 60 Ω/sq n^+ layer on both surfaces without any further cleaning step. Group 1 samples with textured surfaces are afterwards exposed to a H_2O_2/H_2SO_4 cleaning step (Piranha-cleaning) in order to remove organic residues from the texturing process followed by a RCA cleaning for both group 1 and group 2 samples. Directly after the final HF dip, the emitter of these samples is formed by BBr_3 diffusion resulting in a 50 Ω/sq or 100 Ω/sq emitter.

For the solar cells 5 inch 2 Ωcm Cz-Si wafers are used as substrate material and etched to a thickness of approx. 130 µm in NaOH solution before the texturizing process in alkaline solution. The cleaning consists of an HCl step and a subsequent RCA cleaning prior to BBr_3 diffusions for 50 Ω/sq and 100 Ω/sq emitters. Afterwards, a SiN_x capping layer is applied on the front side to protect the emitter on the front side at the subsequent etch back of the emitter on the rear side in NaOH solution and the repeated texturing of the rear side in alkaline solution for an improved electrical contact of the finger grid on the

rear side, leading to a final cell thickness of approx. 100 µm. After cleaning in diluted HCl and HF, a $POCl_3$ diffusion forms the BSF with a sheet resistivity of 60 Ω/sq prior to SiN_x capping layer as well as the PSG being removed in a final HF dip.

The following passivation / ARC stacks or layers are investigated on j_{0e} level:

- ALD Al_2O_3 (5 nm and 15 nm) + r-PECVD SiN_x (thickness optimized as ARC). The remote plasma is expected to decrease the possible damage due to radiation or ions compared to a direct plasma source.
- Dry thermal oxide at 900°C (7 nm and 15 nm) + PECVD SiN_x (optimized thickness)
- Silicon oxide layer resulting from the second RCA step (thickness assumed to be 3 nm) + PECVD SiN_x (optimized thickness)
- 75 nm PECVD SiN_x (only on planar samples)

The solar cells are passivated on front/emitter side and rear side with following passivation layer combinations:

- Al_2O_3 + r-PECVD SiN_x on front side / PECVD SiN_x on rear side
- Thermal SiO_x + PECVD SiN_x on front and rear side
- RCA SiO_x + PECVD SiN_x on front and rear side

These combinations are also used for calculating the combined saturation currents $j_{0combined}$ of front- and rear side.

Metallization of the solar cells is maintained by screen printing of an AgAl paste on the front and an Ag paste on the rear side followed by co-firing in a 9-zone belt firing furnace. As the cells are designed as bifacial cells, a finger grid is printed on both sides instead of a full-area rear side metallization.

j_{0e}/j_{0BSF} values are measured with a Sinton Lifetime Tester WCT-120 on both planar and pyramid textured samples, the complex refractive index (n- and k- values) is determined by ellipsometry using a J. A. Woollam device only on samples with planar surfaces. All parameters are measured after a high temperature step in a firing belt furnace at the same set peak temperatures as for the solar cells.

The SiN_x layer thicknesses are optimized regarding best ARC properties applying a numerical calculation method using the determined n- and k- values of the layers as input parameters.

For the solar cell results the IV curve is measured on a constant light cell tester.

3 RESULTS

In Figure 1 and 2 the j_{0e} values of the investigated layers and stacks are illustrated with a very low j_{0e} of 17.5 fA/cm² for a 15 nm Al_2O_3 + SiN_x stack as passivation layer on a 100 Ω/sq emitter and a planar surface. For most passivation layers, j_{0e} is lower for 100 Ω/sq emitters than for 50 Ω/sq emitters which is expected to be caused by a higher recombination in the 50 Ω/sq emitter bulk and a simultaneously identical recombination at the surface, as both emitters feature similar surface doping concentrations but different profile depths. Furthermore, the results show an increased j_{0e} for samples with textured surfaces which can be referred to the larger surface area of a pyramid textured compared to a planar surface and so to an enhanced surface recombination.

The differences between stacks with 5 nm Al_2O_3 and 15 nm Al_2O_3 or 7 nm SiO_x and 15 nm SiO_x are rather small, suggesting to further decrease the layer thickness, especially of Al_2O_3, and to examine if passivation quality can be maintained. This renders the opportunity to reduce the process duration and to further optimize light trapping when applying an Al_2O_3/SiN_x stack with an Al_2O_3 thickness below 5 nm.

Passivation stacks consisting of RCA SiO_x + SiN_x exhibit the highest j_{0e} values except for the pure SiN_x layer which is only measured on planar surfaces. However, the difference of RCA SiO_x + SiN_x passivated samples to samples passivated with thermal SiO_x + SiN_x is rather small on textured.

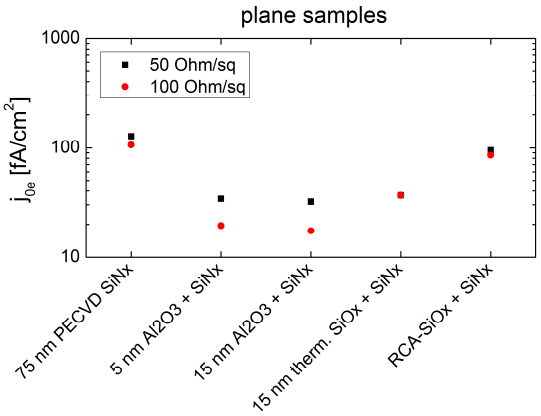

Figure 1: j_{0e} values of BBr_3 diffused samples with planar surfaces and different surface passivations

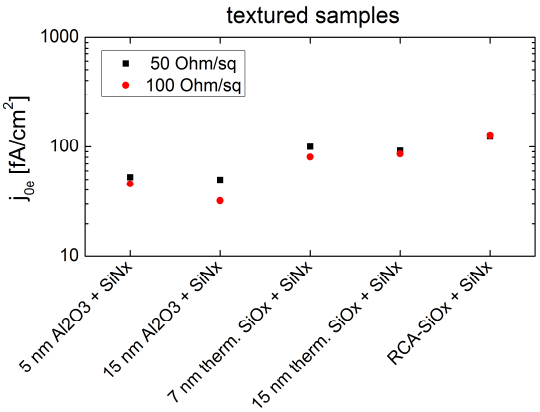

Figure 2: j_{0e} values of BBr_3 diffused samples with textured surfaces and different surface passivations

j_{0BSF} values illustrated in Figure 3 reveal a clearly advanced passivation performance when using a stack consisting of thermal SiO_x + SiN_x compared to a SiN_x single layer. Obviously, a thin interface layer of RCA SiO_x does not have a similar influence on the passivation properties as thermal SiO_x. Compared to the j_{0e} values in Figure 1 and 2, the j_{0BSF} values in Figure 3 are much higher emphasizing the importance of a sophisticated rear side passivation.

For comparing different cell concepts distinguished by their front and rear side design, the saturation current densities of the emitter side and the corresponding BSF side are combined and yields the saturation current

densities $j_{0combined}$ illustrated in Figure 4. Each saturation current density was determined on symmetric samples.

In this calculation, saturation current density of a solar cell base and that caused by an increased recombination at the not passivated area under the metal contacts is not included, as these two saturation current densities are just a constant offset to the overall j_0 values independent of surface passivation layout.

The results reveal the lowest combined saturation current densities to be attained for samples passivated with thermal SiO_x + SiN_x on front and rear, despite the not optimal saturation current density on the emitter side. Highest combined saturation current densities are determined for RCA SiO_x + SiN_x passivation on both sides which is mainly due to the contribution of the j_{0BSF}. For the same reason, the $j_{0combined}$ of samples with Al_2O_3 + SiN_x emitter passivation is higher due to the high j_{0BSF} of the PECVD SiN_x passivated BSF.

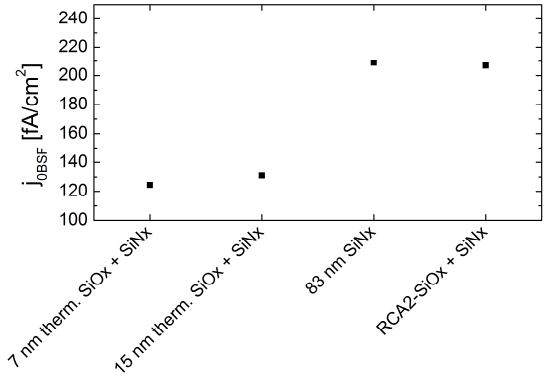

Figure 3: j_{0BSF} values of $POCl_3$ diffused samples on textured surfaces and different surface passivations

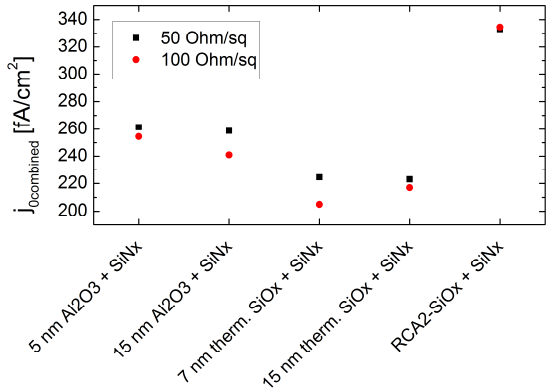

Figure 4: Combined saturation current densities $j_{0combined}$ calculated by adding the j_{0e} of the BBr_3 diffused front side and the corresponding j_{0BSF} of the $POCl_3$ diffused rear side for different passivations. Labeled passivation layers in the graph correspond to the passivation of the emitter side.

The IV characteristics of the solar cells featuring a 50 Ω/sq emitter in Table I confirm the trend of the combined saturation current densities in Figure 4. The highest efficiency of 18.0% is measured for cells with thermal SiO_x + SiN_x passivation followed by the solar cells with Al_2O_3 + SiN_x passivation. SiO_x and Al_2O_3 layer thicknesses have only a negligible influence. Both j_{SC} and V_{OC} and thus cell efficiency are very low for solar cells passivated by RCA SiO_x + SiN_x which also corresponds to the results of the combined saturation current density illustrated in Figure 4.

A different trend is observed for solar cells with 100 Ω/sq emitter in Table II with a maximal efficiency of 17.0% for Al_2O_3 + SiN_x passivation. The efficiency loss for cells with a thermal SiO_x + SiN_x compared to an Al_2O_3 + SiN_x passivation is mainly due to a much lower V_{OC}. As neither the used AgAl pastes nor the firing parameters (except the peak temperatures) are optimized for these cells, a possible explanation for the voltage drop can be found in metallization issues when contacting the very shallow 100 Ω/sq emitter.

Table I: IV characteristics of bifacial n-type solar cells with 50 Ω/sq emitter and 60 Ω/sq BSF for different passivation layers (labeled layers correspond to the front side passivation)

	j_{SC} [mA/cm²]	V_{OC} [mV]	η [%]
5 nm Al_2O_3 + SiN_x	37.1	623	16.7
15 nm Al_2O_3 + SiN_x	36.4	623	16.3
RCA SiO_x + SiN_x	30.5	601	13.4
7 nm SiO_x + SiN_x	37.3	631	18.0
15 nm SiO_x + SiN_x	36.7	632	17.9

Table II: IV characteristics of bifacial n-type solar cells with 100 Ω/sq emitter and 60 Ω/sq BSF for different passivation layers (labeled layers correspond to the front side passivation)

	j_{SC} [mA/cm²]	V_{OC} [mV]	η [%]
5 nm Al_2O_3 + SiN_x	36.3	620	17.0
15 nm Al_2O_3 + SiN_x	37.1	617	17.0
RCA SiO_x + SiN_x	32.3	594	13.9
7 nm SiO_x + SiN_x	36.8	603	15.7
15 nm SiO_x + SiN_x	37.4	610	15.6

In general, a further increase of cell efficiency is expected for an advanced passivation of the solar cell rear side as well as an optimized metallization.

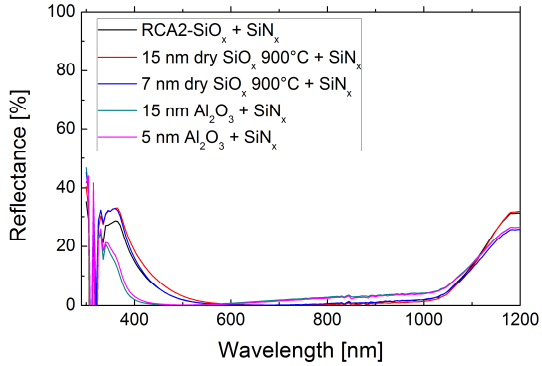

Figure 5: Measured spectral reflectance of the investigated front side passivation layers

The measurements of the complex refractive index by means of ellipsometry in a wavelength range between 290 nm and 1000 nm (results not illustrated here) show that thermal SiO_x and Al_2O_3 are fully transparent in the entire wavelength range. Both PECVD and r-PECVD SiN_x absorb at wavelengths below 400 nm and 450 nm,

respectively, with an increasing absorption coefficient towards shorter wavelengths. All layers exhibit only slight changes of the n- and k- values caused by the firing step.

Figure 5 illustrates the spectral reflectance of the investigated layers in the relevant wavelength range of 290 nm to 1200 nm which in general is very low for all passivation layers. Stacks of $Al_2O_3 + SiN_x$ have a minimum at a smaller wavelength compared to the other stacks exhibiting a lower reflectance over the higher wavelength range. The visible color of all layers is dark blue to black with a purple shade at the $Al_2O_3 + SiN_x$ samples.

4 CONCLUSIONS

The results presented in this work emphasize $Al_2O_3 + SiN_x$ stacks to be best suited to passivate BBr_3 diffused emitters yielding a very low emitter saturation current density of 17.5 fA/cm². However, the high recombination velocity on the SiN_x passivated $POCl_3$ diffused BSF on the rear side limits the performance of the cells. Maximum efficiencies of 18.0% are achieved employing a 50 Ω/sq emitter and a thermal $SiO_x + SiN_x$ passivation stack on both surfaces despite a possible parasitic shunting of the p-n junction described by Dauwe [9] due to the positive fixed charges in the passivation layer. Furthermore, a firing step does not deteriorate the passivation properties of the investigated layers as the emitter saturation current densities still exhibit sufficiently low values.

As spectral reflectance measurements reveal, a very low reflectance over the relevant wavelength region can be achieved using the investigated layers with optimized thickness.

5 ACKNOWLEDGEMENTS

The authors would like to thank L. Kraus and L. Mahlstaedt for their processing assistance. The research leading to these results has received funding from the EU 7th Framework Programme (FP7/2007-2013) for the Collaborative Project (CP) '20plµs' with the full title: ‘Further development of very thin wafer based c-Si photovoltaics' under grant agreement n° 256695. The content of this publication is the responsibility of the authors.

6 REFERENCES

[1] J. Zhao, A. Wang, P.P. Altermatt, M.A. Green, J.P. Rakotoniaina, O. Breitenstein, Proc. 29th IEEE PVSC, New Orleans, USA (2002) 218.
[2] F. Kiefer, C. Ulzhöfer, T. Brendemühl, N.-P. Harder, R. Brendel, V. Mertens, S. Bordihn, C. Peters, J.W. Müller, IEEE J. Photov. 1 (1) (2011) 49.
[3] J. Benick, B. Hoex, M.C.M. van de Sanden, W.M.M. Kessels, O. Schultz, S.W. Glunz, Appl. Phys. Lett. 92 (2008) 253504.
[4] W. Kern, D. Poutinen, RCA Review 31 (1970) 187.
[5] D. Macdonald, L.J. Geerlings, Appl. Phys. Lett. 85 (2004) 4061.
[6] V.V. Voronkov, R. Falster, J. Appl. Phys. 107 (2010) 053509.
[7] Y. Schiele, S. Fahr, S. Joos, G. Hahn, B. Terheiden, this conference.
[8] D. E. Kane, R. M. Swanson, Proc. 18th IEEE PVSC, Las Vegas, USA (1985) 578.
[9] S. Dauwe, L. Mittelstädt, A. Metz, R. Hezel, Progr. Photovolt. 10 (2002) 271.